Photoelectron spectra from local-density-functional calculations: Application to chain polymers

J. W. Mintmire, F. W. Kutzler,* and C. T. White
Naval Research Laboratory, Washington, D.C. 20375-5000
(Received 6 March 1987)

We describe a computational method for calculating valence-photoelectron line shapes for chain polymers and building blocks of chain polymers. This method is based on local-density-functional calculations that generate molecular orbitals (or Bloch orbitals) from linear combinations of atom-centered products of radial functions and spherical harmonics. Comparisons between theoretical predictions and experimental photoelectron spectra for a range of chain polymers and metal-phthalocyanine systems are reported and discussed. These comparisons demonstrate the success and the wide applicability of our approximate one-electron scheme.

INTRODUCTION

X-ray (XPS) and ultraviolet (UPS) photoelectron spectroscopy provide powerful experimental probes of the valence spectra of molecules, polymers, and solids. Results of theoretical electronic structure calculations are often compared to these spectra, both to understand the features observed and to test the calculations. Construction of a theoretical XPS or UPS line shape requires the knowledge of the appropriate excitation energies of the sample ground state and the cross sections for all such excitations. However, for large systems, the effects of varying cross sections across the valence spectra are often neglected in the theoretical results; direct comparisons are made simply between the calculated one-electron spectrum and the XPS and UPS experimental results. This approximation is not severe for some systems[1] where good agreement has been obtained between the predicted density-of-states (DOS) and the XPS line shape. On the other hand, the effects of varying cross sections across the valence spectra are important in understanding the XPS and UPS line shapes of a number of chain polymers that have been studied because of either their semiconducting, dielectric, or piezoelectric behavior. These materials range from the relatively simple chain polymers such as polyacetylene to the much more complex ones formed by stacking metal-phthalocyanine units. As noted by Delhalle,[2] for such materials a direct comparison between the DOS and the XPS line shape becomes difficult and unsatisfactory. To overcome this difficulty, Delhalle *et al.*, following Gelius,[3] weighted their *s*- and *p*-orbital DOS by different empirical cross sections. This approach clearly improved agreement between theory and experiment but at the cost of additional parametrization.

In an earlier work[4] we described a method for calculating XPS and UPS line shapes for polyacetylene from local-density-functional (LDF) electronic structure calculations using Hermite-Gaussian basis sets. This method used the wave functions from the LDF calculations along with time-dependent perturbation theory to calculate the photoelectron line shapes. Other than the usual normalization of the total integrated valence intensity and the alignment of experimental and theoretical thresholds, no parameters entered this approach. The method, however, does not include relaxation effects, molecular-potential effects on the outgoing free-electron state, and other such corrections. Nevertheless, for polyacetylene, we obtained good agreement between the theoretically predicted and experimentally measured XPS and UPS line shapes. Recently we have demonstrated that this computational approach can be generalized from LDF calculations using Hermite-Gaussian basis sets to any LDF calculation for an infinite or large finite system so long as the one-electron wave functions can be expressed as linear combinations of atom-centered products of radial functions and spherical harmonics.

Below we first outline the general method. Next, we demonstrate the success of this approach by comparison of predicted theoretical results with experimental results for a number of chain polymers and metal-phthalocyanine systems which can be building blocks for chain polymers.

FORMALISM

We use LDF theory in combination with methods[5–7] long used to estimate photoelectron cross sections for small molecules to calculate the photoelectron line shapes of infinite chain polymers and large molecules such as the phthalocyanines. First-order time-dependent perturbation theory and a semiclassical description of the radiation-matter interaction are used to calculate the cross sections necessary to describe the photoelectron spectra. Within this approach, the differential cross section for bound-to-free transitions from an initial state, u_i, to a final state, u_f, induced by incident radiation of angular frequency ω and averaged over polarization and direction of incidence is given by[8]

$$\frac{d\sigma}{d\Omega}=\frac{e^2L^3k_f}{6\pi mc\omega}\,|\,\mathbf{P}\,|^2\,, \tag{1}$$

where L is the edge length of a large but finite cubic box used to normalize the continuum function, and the transition matrix element $\mathbf{P}$ is defined as

$$\mathbf{P}=\int d^3r\, u_f(\mathbf{r})\nabla u_i(\mathbf{r})\,. \tag{2}$$

Following earlier workers,[5-7] we approximate the final outgoing state u_f with a plane wave:

$$u_f(\mathbf{r}) = \exp(-i\mathbf{k}_f\cdot\mathbf{r}) , \tag{3}$$

where $\mathbf{k}_f$ defines the momentum, $\hbar\mathbf{k}_f$, of the outgoing plane wave representing u_f. This final-state wave vector must conserve total energy such that $\hbar^2k_f^2/2m = \hbar\omega + \varepsilon_i$, where ε_i is the energy of the one-electron initial state u_i. Using Eqs. (2) and (3) and the anti-Hermitian nature of the gradient operator, we can express $|\mathbf{P}|^2$ defined by Eq. (2) as

$$|\mathbf{P}|^2 = k_f^2 \left| \int d^3r\, u_i(\mathbf{r}) \exp(i\mathbf{k}_f\cdot\mathbf{r}) \right|^2 . \tag{4}$$

A plane wave is the simplest approximation for the final-state wave function. Systematic and computationally feasible improvements can be made to this approximation by using an orthogonalized plane wave[7] with more and more inner states (both occupied and unoccupied) included in the orthogonalization procedure. For the range of systems studied in this paper, however, we find good agreement between theory and experiment without introducing these additional complications into the formalism and associated calculations. Although the plane-wave approximation will be better far from threshold and hence better for XPS than UPS, we nevertheless find good agreement between theory and experiment for both XPS and UPS in the systems studied.

In our approach the wave functions $u_i(\mathbf{r})$ and the corresponding eigenvalues ε_i, necessary to evaluate Eq. (4), are obtained by solving the LDF equations,[9]

$$(-\tfrac{1}{2}\nabla^2 + V_C + V_{\rm xc})u_i = \varepsilon_i u_i , \tag{5}$$

where the Coulomb potential, V_C, includes both the electron-nuclear attractive interaction and the classical electron-repulsion term, and $V_{\rm xc}$ denotes the exchange-correlation potential. Throughout we assume the Gáspar-Kohn-Sham[9,10] form for $V_{\rm xc}$.

Because V_C and $V_{\rm xc}$ both depend on the electron density $\rho(\mathbf{r})$, the differential equations (5) must be solved self-consistently. Several linear combination of nuclear-centered-functions methods[11,12] have been developed to solve these equations. A common feature of these methods is that they lead to self-consistent solutions of the form

$$u_i(\mathbf{r}) = \sum_{p,l,m} C_{plm}\phi_{plm}(\mathbf{r}-\mathbf{R}_p) , \tag{6}$$

where ϕ_{plm} denotes a function centered about the nuclear position $\mathbf{R}_p$ and having the form

$$\phi_{plm}(\mathbf{r}-\mathbf{R}_p) = f_{plm}(\mathbf{r}-\mathbf{R}_p)Y_{lm}(\hat{r}) . \tag{7}$$

In Eqs. (7), f_{plm} is a radial function and Y_{lm} denotes a spherical harmonic. Note that the functions ϕ_{plm} do not refer to a primitive basis function in a typical linear combination of atomic orbitals (LCAO) scheme, but rather the contribution of all primitive basis functions with the form of Eq. (7) and given value of l and m centered about nuclear site p for the initial state (i.e., molecular orbital) u_i. For wave functions of the form expressed in Eq. (6) and (7), we show in the Appendix for the angularly averaged spectrum that Eq. (4) can be reduced to

$$|\mathbf{P}|^2 = 4\pi k_f^2 \sum_{p,l,m} |C_{plm}|^2 |X_{plm}(k_f)|^2 , \tag{8}$$

where

$$X_{plm}(k_f) = \int_0^\infty j_l(k_f r) f_{plm}(r) r^2 dr , \tag{9}$$

with j_l a Bessel function. We use this result for $|\mathbf{P}|^2$ to calculate the XPS and UPS line shapes from Eq. (1). Equations (8) and (9) can be used with any method assuming wave functions of the form defined by Eqs. (6) and (7). In our approach the LDF equation (5) is used to determine these wave functions for all initial states.

RESULTS

We have applied the approach outlined in the previous section to a broad array of chain polymers and large molecular systems. Below we present some representative results which are compared with experiment.

A. Polyacetylene

All-*trans*-polyacetylene (PA), made up of planar chains such as shown in Fig. 1(a), is considered the prototypical wide-band quasi-one-dimensional semiconducting polymer. In an earlier[13] wide-ranging theoretical study of the properties of this system we reported LDF-based results for the XPS and UPS of polyacetylene that were in good agreement with experiment. No detailed discussion of the various features present in the line shape was given, however. Therefore, we begin by first discussing in greater detail these previous results.

Calculated photoelectron PA valence line shapes for incident photon energies of 40.8 eV (UPS) and 1254 eV (XPS) are shown in Fig. 2. The wave functions, u_i and one-electron eigenvalues, ε_i, necessary to calculate these spectra were obtained from the LCAO-LDF chain polymer program.[13] A $7s3p$ Gaussian basis was used to de-

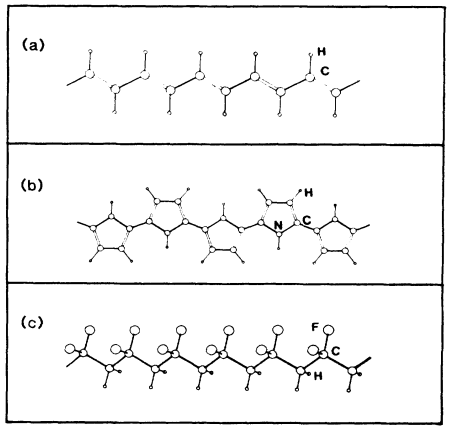

FIG. 1. (a) Polyacetylene, (b) polypyrrole, and (c) polyvinylidene fluoride chains.

scribe the carbon sites and a 3*s* basis set was used to describe the hydrogen sites. The PA chain geometry was chosen by constraining all bond angles to 120°, setting the C—H bond lengths to 1.08 Å, and fixing the C—C single and double bond lengths at 1.45 Å and 1.35 Å, respectively.

Also shown in Fig. 2 are experimental results for the XPS and UPS spectra of PA. The XPS spectrum was taken by Brundle[14] and the UPS spectrum by Salaneck *et al.*[15] To compare theory with experiment both the integrated theoretical XPS and UPS intensities were normalized. The experimental XPS absorbtion edge was also shifted to match the theoretical threshold and the UPS data was aligned with the theoretical results assuming a work function of 4.5 eV. As can be seen from Fig. 2, if a straight-line background subtraction of the experimental data is assumed, good agreement between the experimental and theoretical line shapes is found for both the XPS and UPS spectra. The major XPS peak at −17 eV originates from carbon 2*s* states. In chemical terms these states together with carbon 2*p* states form C—C σ bonds which are broadened into bands because of their interactions along the PA chain. These bands' contribution to the XPS spectra extends from about −18 to −8 eV. Below −15 eV almost all contribution to the XPS and UPS spectra are from these C—C bonds which become progressively more *p* like with increasing energy. At about −12 eV these states mix strongly with states from C—H bonds which extend from about −14 to about −5 eV. These mixed states, with a major contribution from C—H bonds, produce the second peak in the XPS spectra at about −12 eV. Although of relatively small measure, this peak is also resolved in the theoretical and experimental UPS spectra in Fig. 2.

The most pronounced peak in both the experimental and theoretical UPS spectrum occurs close to −7 eV. This peak arises principally from carbon $2p\pi$ orbitals which form a band of occupied states extending from a little below −7 eV to threshold. The accumulation of these states at the lower $2p\pi$ band edge produces the major observed peak in the UPS spectrum. This major peak in the UPS spectrum also exhibits a high-energy shoulder that is discernible in both the experimental and theoretical results. This shoulder, occurring at approximately −5 eV, has a large contribution from antibonding combinations of C—H bonding orbital. No occupied σ orbitals occur above −5 eV. Comparing the DOS for PA shown in Fig. 2(a) to the theoretically predicted XPS and UPS spectra demonstrates the importance of including cross-section effects in analyzing these spectra.

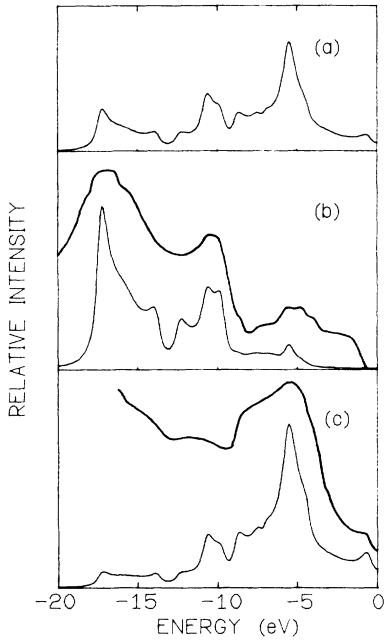

FIG. 2. (a) DOS for all-*trans*-polyacetylene, (b) theoretical and experimental XPS spectra for *trans*-polyacetylene, and (c) theoretical and experimental UPS spectra for *trans*-polyacetylene. Upper lines in (b) and (c) represent experimental results and lower lines represent theoretical results. No background subtraction has been made for the experimental results.

B. Polypyrrole

Like polyacetylene, polypyrrole (PP), composed of planar chains such as shown in Fig. 1(b), is another example of a quasi-one-dimensional semiconducting polymer that has been extensively studied.[16] Although the valence XPS of this material has not been reported, valence UPS results have.[17] Figure 3 shows a comparison of our calculated UPS spectra to those experimental results. As with polyacetylene, this comparison is made by aligning thresholds, normalizing the total integrated intensity, and using the self-consistent LCAO-LDF method for chain polymers[13] to obtain the wave functions, u_i, and one-electron energy eigenvalues necessary to evaluate Eq. (4).

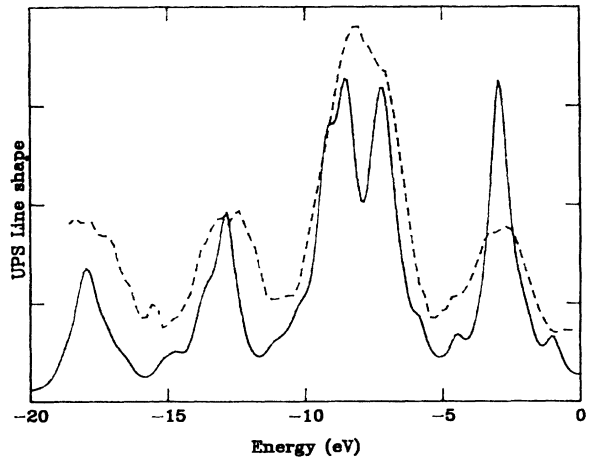

FIG. 3. Theoretical (solid line) and experimental (dashed line) UPS spectra (40.8 eV incident photon energy) of polypyrrole. Energy scale is relative to the Fermi level. Theoretical results have been broadened with a 0.7-eV full width at half maximum Gaussian. Because of the extremely steep rising background, a straight-line background subtraction has been made on the experimental results.

The geometry of PP used in these calculations was chosen by optimizing the bond lengths and bond angles with the modified neglect of diatomic overlap (MNDO) method[18] for a cluster of five pyrrole units linked at the α, α' locations and constrained to be planar.[19] This choice of conformation is in agreement with experimentally suggested conformations.[20] A $4s2p$ Gaussian basis set was used for the carbon and nitrogen sites, and a $2s$ basis was used for the hydrogen sites.[21]

The peak in Fig. 3 at about -3 eV originates from the π orbitals in the PP chain, with the sharpness of the peak at -3 eV caused by a flat π band with a major contribution from the nitrogen nonbonding $2p$ state. The energy level of this p state should be sensitive to local bond-length changes and other such local effects; such effects might account for the lack of sharpness in the corresponding experimental peak. The intense peaks at about -8 eV arise from the σ orbitals with contributions from carbon and nitrogen $2p$ and $2s$ orbitals, and hydrogen $1s$ orbitals, while the peak at -13 eV has major contributions from the carbon and nitrogen $2s$ orbitals. The peaks at -18 eV and -23 eV arise from the carbon and nitrogen $2s$ states, respectively, with some mixing of different type states and with broadening due to band width.

Other workers have recently used Hartree-Fock methods to calculate the electronic structure of PP (Ref. 22) and compared their resultant DOS with the experimental UPS results.[17] Comparing these results with ours, one notes two major differences.

(1) The Hartree-Fock eigenvalue spectrum and resulting peak locations are more widely spaced in energy than either our results or experiment suggests.

(2) The relative peak heights and shapes of the Hartree-Fock DOS are not in as good agreement with experiment as our results, suggesting the importance of including photoemission cross-section effects in this type of chain polymer.

C. Polyvinylidene fluoride

Although formed from carbon backbone chains as are polyacetylene and polypyrrole, polyvinylidence fluoride (PVDF), is not semiconducting but rather a good insulator because of its tetrahedral bond structure. In addition, because of the strong electronegativity of fluorine this material can possess large permanent dipole moments and can exhibit an intense piezoelectric response. This piezoelectric behavior has stimulated much interest in this polymer. Its tetrahedrally bonded, highly polarized character makes PVDF quite different from PA and PP and as such an excellent further test of our methods.

LCAO-LDF calculations were performed for PVDF using the regular zigzag chain conformation with all carbons coplanar and with perfect tetrahedral bond structure about the carbon atoms. Bond distances used[23] were 1.54 Å for carbon–carbon bonds, 1.39 Å for carbon–fluorine bonds, and 1.08 Å for carbon–hydrogen bonds. The basis sets used for these calculations were $8s4p$ for carbon and fluorine and $4s1p$ for hydrogen. Figure 4 depicts a comparison of our calculated XPS spectra with experimental results.[23]

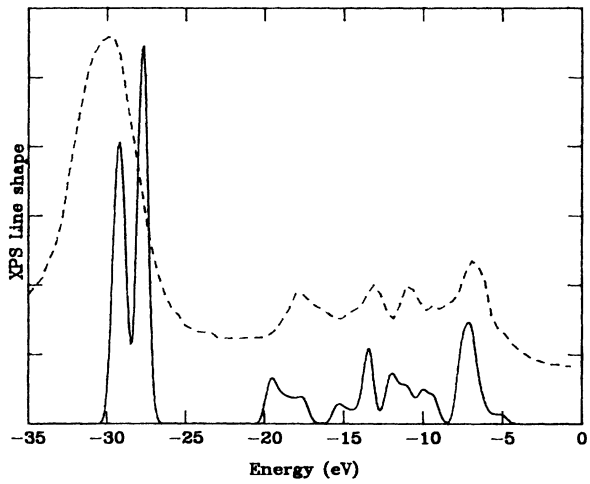

FIG. 4. Theoretical (solid line) and experimental (dashed line) XPS spectra (1480 eV incident photon energy) of polyvinylidene fluoride. Energy scale is relative to vacuum. Theoretical results have been broadened with a 0.7-eV full width at half maximum Gaussian. The experimental results have been background subtracted.

The XPS peak at -29 eV derives from the fluorine $2s$ symmetric and antisymmetric orbitals; the peak at roughly -19 eV derives primarily from carbon $2s$ bonding orbitals. The structure spanning the region from -16 eV to about -9 eV has contributions from carbon $2s$ orbitals (in the lower energy portion of this interval), C—H, and C—F bonds. All of the above results are in good agreement with experimental assignments and earlier theoretical results[23] based on extended Hückel crystal orbital (EHCO) methods. These earlier EHCO results also predicted that the fluorine $2p$ nonbonding states would generate a large peak several eV below the XPS threshold. The experimental results, however, indicate that these states produce a rather well defined peak at about -7 eV occurring at the leading edge of the XPS line shape. Our peak at about -7 eV arises in large part from the fluorine $2p$ states—in agreement with experimental assignments.

D. Phthalocyanines

The phthalocyanine (Pc) molecule and related metal-Pc complexes, such as shown in Fig. 5, are of interest to us because of the electrically conductive behavior of the quasi-one-dimensional materials obtained by iodine doping partially oxidized metal-phthalocyanines stacks.[24] The electronic structure of phthalocyanine compounds, however, are of interest also because of their catalytic properties[25] and because they are related to biologically important porphyrins such as chlorophyll and hemoglogin. These molecules provide an additional test for our methods, because in contrast to the systems treated so far, they contain a finite number of atoms and can include transition metals.

The photoelectron spectra of the phthalocyanines

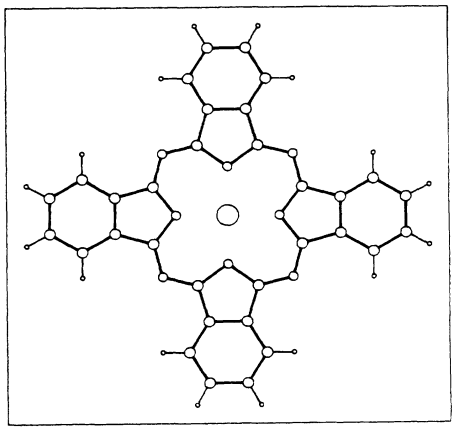

FIG. 5. Metal-phthalocyanine molecule. Hydrogen, nitrogen, and carbon atoms are shown as onefold, twofold, and threefold coordinated, respectively. The centrally located sphere depicts the metal atom.

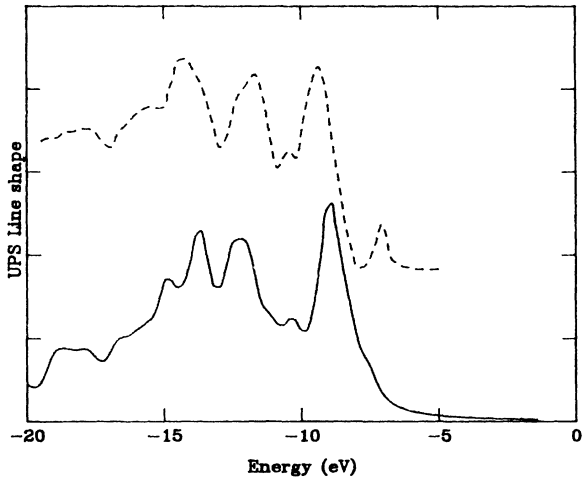

FIG. 6. Theoretical (solid line) and experimental (dashed line) UPS spectra (40.8-eV incident photon energy) of H_2-Pc. Energy scale is relative to vacuum. Theoretical results have been broadened with a 0.5-eV full width at half maximum Gaussian. The experimental results have not been background subtracted.

were computed from self-consistent molecular orbitals obtained by using the discrete variational method (DVM) (Ref. 12) to solve the LDF equations. The molecular orbitals in this technique are constructed from linear combinations of numerical orbitals which are one-electron wave functions of the neutral isolated atoms, calculated within the DVM model. Below we compare theoretical photoelectron spectra with experimental results for the metal-free phthalocyanine (H_2Pc) and for the copper-phthalocyanine (Cu-Pc) complex. Molecular geometries in all calculations were taken from crystallographic studies.[26,27] Once again in comparing experiment to theory thresholds were aligned and integrated intensities normalized. Figure 6 depicts a comparison of our theoretically calculated UPS spectrum for H_2-Pc with the experimental results.[28] Agreement with experiment is good, with the exception of a small peak in the experimental results just below threshold at about -7 eV. This peak might signal dynamic effects not present in a one-electron model.

An unambiguous classification of peaks by atomic origin is impossible for the UPS spectrum of H_2-Pc because of the diversity of electronic environments within the phthalocyanine molecule and because of the large number of transitions which make up each peak. Nevertheless, a few generalizations can be made. The major peaks in Fig. 6 are from carbon and nitrogen p orbitals. The peak falling slightly above -10 eV (representing the orbitals of lowest binding energy) primarily arises from a number of pp-π bonding orbitals, although this region also includes nitrogen lone-pair orbitals. The two peaks and their side lobes lying roughly between -12 and -14 eV are mostly from pp-σ bonding orbitals. This region also contains some particularly low-energy pp-π orbitals bonding the α-carbons to the nitrogens on either side. Peaks below -14 eV are entirely due to pp-σ bonding, and have greater hybridization with carbon and nitrogen $2s$ states than do orbitals at higher energies. The weak peaks caused by s-dominated orbitals lie at still lower energies and are not shown.

Figure 7 depicts our results for the XPS of Cu-Pc, which are also in good agreement with the experimental results.[28] The theoretical (as well as experimental) UPS for the metal-Pc complexes are all similar to each other. Figure 7 emphasizes the importance of including transition cross sections in calculating the photoelectron spectra line shapes. At the high photon energy (1487 eV)

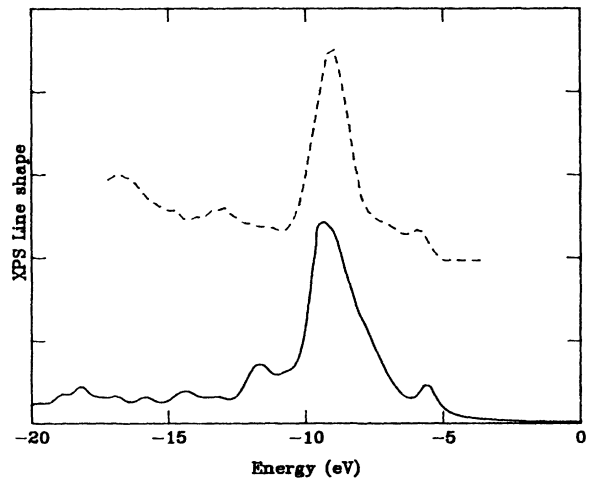

FIG. 7. Theoretical (solid line) and experimental (dashed line) XPS spectra (Al $K\alpha$ line, 1487-eV incident photon energy) of Cu-Pc. Energy scale is relative to vacuum. Theoretical results have been broadened with a 0.5-eV full width at half maximum Gaussian. The experimental results have not been background subtracted.

which gives the Cu-Pc XPS spectrum in Figure 7, only transitions involving copper $3d$ orbitals have an appreciable relative cross section. The molecular orbitals dominated by the Cu $3d$ states lie at energies between -8 and -10 eV, and so produce the major peak. The small peak of highest energy is caused by ionization from the half-filled Cu $d_{x^2-y^2}$ orbital at about -5.5 eV. The side lobe at about -12 eV is due to Cu $d_{(xz,yz)}$ character mixed with ring π-bonding molecular orbitals.

SUMMARY

We have presented a procedure for calculating photoelectron spectra from LDF electronic structure calculations which use molecular or Bloch orbitals constructed from linear combinations of atom-centered products of radial functions and spherical harmonics. Once solutions to the LDF equations have been obtained in terms of such orbitals the additional computational steps necessary to implement this method are straightforward. This scheme is not restricted to the chain polymers and related systems treated herein but is perfectly general and should be applicable to other systems as well. The energy of the incident photon is part of the input to the procedure, which allows results for both UPS and XPS. We have presented results using electronic structure calculations from two types of local-density-functional calculations: one using Gaussian basis sets and the other using numerical basis sets. Both sets of results yield theoretical photoelectron line shapes in good agreement with experiment.

ACKNOWLEDGMENTS

F. W. Kutzler thanks the National Research Council for support through a National Research Council–Naval Research Laboratory program. This work was supported by the Office of Naval Research.

APPENDIX

Using wave functions of the form defined in Eqs. (6) and (7), we can rewrite the integral in Eq. (4) as

$$\begin{aligned}\int d^3r\, u_i(\mathbf{r})\exp(i\mathbf{k}_f\cdot r) &= \sum_{p,l,m} C_{plm}\exp(i\mathbf{k}_f\cdot\mathbf{R}_p)\int d^3r\, f_{plm}(r)Y_{lm}(\hat{r})\exp(i\mathbf{k}_f\cdot\mathbf{r}) \\ &= \sum_{p,l,m} C_{plm}\exp(i\mathbf{k}_f\cdot\mathbf{R}_p)\int d^3r\, f_{plm}(r)Y_{lm}(\hat{r})\left[4\pi\sum_{l',m'} i^{l'}j_{l'}(k_f r)Y_{l'm'}(\hat{r})Y^*_{l'm'}(\hat{\mathbf{k}}_f)\right] \\ &= 4\pi\sum_{p,l,m} i^l C_{plm}\exp(i\mathbf{k}_f\cdot\mathbf{R}_p)X_{plm}Y_{lm}(\hat{\mathbf{k}}_f)\ , \end{aligned} \tag{A1}$$

where the last two expressions use the standard expansion of the plane wave in spherical harmonics and X_{plm} is defined by Eq. (9). Typically experimental photoelectron spectroscopy results are not angularly resolved and this produces averages over all allowed orientations of $\mathbf{k}_f$. Therefore, in our computational scheme we also want a spherical average over all possible orientations of $\mathbf{k}_f$. Using Eq. (A1) to take the spherical average of Eq. (4) yields

$$\int d\Omega\,|\mathbf{P}|^2 = 4\pi k_f^2\sum_{p,l,m}\sum_{p',l',m'} i^{(l-l')}C^*_{plm}C_{p'l'm'}X^*_{plm}(k_f)X_{p'l'm'}(k_f)\int_\Omega d\hat{\mathbf{k}}_f\exp(i\mathbf{k}_f\cdot\mathbf{D}_{pp'})Y^*_{lm}(\hat{\mathbf{k}}_f)Y_{l'm'}(\hat{\mathbf{k}}_f)\ , \tag{A2}$$

where $\mathbf{D}_{pp'}=\mathbf{R}_p-\mathbf{R}_{p'}$. Expanding the plane wave in spherical harmonics, we then find that

$$\int_\Omega d\hat{k}_f\exp(i\mathbf{k}_f\cdot\mathbf{D}_{pp'})Y^*_{lm}(\hat{k}_f)Y_{l'm'}(\hat{k}_f) = 4\pi\sum_{l'',m''} i^{l''}j_{l''}(k_f D_{pp'})Y_{l''m''}(\hat{D}_{pp'})\int_\Omega d\hat{k}_f Y^*_{lm}(\hat{k}_f)Y_{l'm'}(\hat{k}_f)Y_{l''m''}(\hat{k}_f)\ . \tag{A3}$$

Next we note that for typical internuclear spacings and incident photon energies, the argument of the Bessel function in Eq. (A3) will be more than an order of magnitude greater than unity unless the nuclear positions $\mathbf{R}_{p'}$ and $\mathbf{R}_p$ are identical. We can thus estimate the value of the Bessel function using the limiting values

$$\lim_{r\to\infty} j_l(r)\to\frac{1}{r}\cos\left[r-\frac{(l-1)\pi}{8}\right] \tag{A4}$$

and

$$j_l(0)=\delta_{0l}\ . \tag{A5}$$

The cross sections defined using Eq. (4) could be calculated directly using Eq. (A3) by evaluating both the Bessel functions and integrals over spherical harmonics, which are Gaunt coefficients. We find, however, that we can neglect all terms in Eq. (A3) for which the nuclear positions differ. This approximation is reasonable because the Bessel functions will have small magnitudes for $p\neq p'$, the magnitudes of the Gaunt coefficients will be less than unity, and the number of nonzero terms over l'' and m'' will be finite. Given the above approximations, Eq. (4) then reduces to Eq. (8).

*Present address: Department of Chemistry, Tennessee Technological University, Cookeville, Tennessee 38505.

[1]For a review containing such results see L. Ley, M. Cardona, and R. A. Pollak, *Topics in Applied Physics,* edited by L. Ley and M. Cardona (Springer-Verlag, New York, 1979), pp. 12–172.

[2]J. Delhalle, S. Delhalle, and J.-M. André, Chem. Phys. Lett. **34**, 430 (1975).

[3]U. Gelius, *Electron Spectroscopy,* edited by D. A. Shirley (North-Holland, Amsterdam, 1972), pp. 311–334.

[4]J. W. Mintmire and C. T. White, Int. J. Quantum Chem. S **17**, 609 (1983).

[5]S. Basu, Theor. Chim. Acta **3**, 238 (1965).

[6]I. G. Kaplan and A. P. Markin, Opt. Specktrosk. **24**, 884 (1968) [Opt. Spectrosc. (USSR) **24**, 475 (1968)].

[7]L. L. Lohr, Jr. and M. B. Robin, J. Am. Chem. Soc. **92**, 724 (1970).

[8]K. Smith, *The Calculation of Atomic Collision Processes* (Wiley-Interscience, New York, 1971).

[9]W. Kohn and L. J. Sham, Phys. Rev. **140**, A1133 (1965).

[10]R. Gáspár, Acta Acad. Sci. Hung. **3**, 263 (1954).

[11]B. I. Dunlap, J. W. D. Connolly, and J. R. Sabin, J. Chem. Phys. **71**, 3396 (1979); **71**, 4993 (1979).

[12]D. E. Ellis and G. S. Painter, Phys. Rev. B **2**, 2887 (1970).

[13]J. W. Mintmire and C. T. White, Phys. Rev. B **28**, 3283 (1983).

[14]Results of C. R. Brundle as reported by P. M. Grant and I. P. Batra, Solid State Commun. **29**, 225 (1979); Synth. Met. **1**, 193 (1979/80).

[15]W. R. Salaneck, H. R. Thomas, R. W. Bigelow, C. B. Duke, E. W. Plummer, A. J. Heeger, and A. G. MacDiarmid, J. Chem. Phys. **72**, 3674 (1980); W. K. Ford, C. B. Duke, and A. Paton, *ibid.* **77**, 4564 (1982); W. R. Salaneck (private communication).

[16]K. K. Kanazawa, A. F. Diaz, R. H. Geiss, W. D. Gill, J. F. Kwak, J. A. Logan, J. F. Rabolt, and G. B. Street, J. Chem. Soc. Chem. Commun., 578 (1977).

[17]W. K. Ford, C. B. Duke, and W. R. Salaneck, J. Chem. Phys. **77**, 5030 (1982).

[18]M. J. S. Dewar and W. Thiel, J. Am. Chem. Soc. **99**, 4899 (1977).

[19]C. T. White, J. W. Mintmire, and M. L. Elert (unpublished).

[20]K. K. Kanazawa, A. F. Diaz, W. D. Gill, P. M. Grant, G. B. Street, G. P. Gardini, and J. F. Kwak, Synth. Met. **1**, 329 (1979/80).

[21]F. B. van Duijneveldt, IBM Report No. RJ945, 1971 (unpublished).

[22]J.-M. André, D. P. Vercauteren, G. B. Street, and J.-L. Bredas, J. Chem. Phys. **80**, 5643 (1984).

[23]J. Delhalle, S. Delhalle, J.-M. André, J. J. Pireaux, J. Riga, R. Caudano, and J. J. Verbist, J. Electron Spectrosc. Relat. Phenom. **12**, 293 (1977).

[24]T. J. Marks, K. F. Schoch, Jr., and B. R. Kundalkar, Synth. Met. **1**, 337 (1979/80).

[25]For a review, see A. B. P. Lever, Adv. Inorg. Chem. Radiochem. **7**, 115 (1965).

[26]C. J. Brown, J. Chem. Soc. A 2488 (1968).

[27]C. J. Schram. R. P. Scaringe, D. R. Stojakovic, B. M. Hoffman, J. A. Ibers, and T. J. Marks, J. Am. Chem. Soc. **102**, 6702 (1982).

[28]F. L. Battye, A. Goldman, and L. Kasper, Phys. Status Solidi B **80**, 425 (1977).